Appl. Phys. B 74, 407–414 (2002)
DOI: 10.1007/s003400200818

Applied Physics B
Lasers and Optics

M. JAZBINŠEK✉
M. ZGONIK

Material tensor parameters of $LiNbO_3$ relevant for electro- and elasto-optics

Faculty of Mathematics and Physics, University of Ljubljana and 'J. Stefan' Institute, Jamova 39, Ljubljana, 1000 Slovenia

Received: 4 January 2002/Revised version: 1 February 2002
Published online: 14 March 2002 •

ABSTRACT The complete set of self-consistent parameters of nominally undoped $LiNbO_3$ crystals of congruent composition that describe the electro-optic, piezoelectric, elasto-optic, elastic, and dielectric response has been determined by numerically evaluating available measurements. The parameters were determined at room temperature and consist of the low-frequency clamped dielectric constants ε_{ij}^S, elastic stiffness constants at constant electric field C_{ijkl}^E, piezoelectric stress coefficients e_{ijk}, elasto-optic constants at constant electric field p_{ijkl}^E, and clamped electro-optic coefficients r_{ijk}^S. It is shown that the complete set is required for calculating the effective electro-optic coefficients and dielectric constants in photorefractive applications of $LiNbO_3$.

PACS 42.70.Nq; 77.84.Dy; 78.20.-e

1 Introduction

In the last few decades, lithium niobate has become one of the most important ferroelectric materials because of the richness of its physical properties. It is widely used for elastic and elasto-optic devices due to the large electromechanical coupling coefficients. In optoelectronics and nonlinear optics its large electro-optic and nonlinear optical coefficients are appreciated. As a photorefractive material, lithium niobate is a most promising candidate for long-term photorefractive applications such as holographic data storage. In most of the applications, a complete knowledge of the involved material parameters is of essential importance.

In a photorefractive experiment, where the elastic deformations are associated with a periodic space-charge field, the effective electro-optic coefficients are modified due to inhomogeneity of the electric field [1–3]. In addition to the refractive indices and the clamped (strain-free) electro-optic coefficients r_{ijk}^S, the tensor of the elastic constants at constant electric field C_{ijkl}^E, the piezoelectric stress tensor e_{ijk}, and the elasto-optic (Pockels) tensor at constant electric field p_{ijkl}^E are needed in order to calculate the effective electro-optic coefficients that describe the optical indicatrix change under the influence of the electric-field grating.

The importance of the elasto-optic contributions to the photorefractive effect was practically demonstrated in $KNbO_3$ and $BaTiO_3$ [4–7]. Lithium niobate has been extensively studied for electro- and elasto-optic applications; therefore all the mentioned material parameters are already available in the literature [8, 9]. There are, however, inconsistencies when comparing data from different sources and considering thermodynamic relations between various material parameters. Recent results [10, 11] also showed that extrinsic impurities and deviations of the crystal composition from stoichiometry may slightly influence the material parameters.

We have re-evaluated various measurements from the literature to obtain a set of consistent material parameters that describe the electro-elasto-optic response of a $LiNbO_3$ crystal of congruent composition. Using the new set of parameters we calculate the effective electro-optic coefficients and effective dielectric constant in the interaction planes that coincide with crystallographic planes.

2 Determination of the complete set of material parameters

2.1 *Elastic, piezoelectric, and dielectric properties*

At room temperature, lithium niobate is a trigonal $3m$ ferroelectric material. We use the coordinate system with the z axis aligned in the direction of the spontaneous polarization and the y axis that lies in the mirror-symmetry plane. The sense of the $+y$ direction is determined so that upon compression in the y direction the $+y$ face becomes negatively charged.

The response of a piezoelectric crystal to external electrical and mechanical fields is as usual described with linearised equations. The stress $\underline{\boldsymbol{T}}$ is related to the elastic strain $\underline{\boldsymbol{S}}$ through the elastic effect and to the electric field $\boldsymbol{E}$ through the piezoelectric effect as [12]

$$T_{ij} = C_{ijkl}^E \, S_{kl} - e_{kij} \, E_k \,, \tag{1}$$

where $\underline{\boldsymbol{C}}^E$ is the tensor of the elastic constants at constant electric field or elastic stiffness, and $\underline{\boldsymbol{e}}$ is the piezoelectric stress

✉ *Present address*: Institute of Quantum Electronics, Swiss Federal Institute of Technology, ETH Hönggerberg, HPF-E12, 8093 Zürich, Switzerland
Fax: +41-1/633-1056, E-mail: mojca@fiz.uni-lj.si

tensor. The dielectric response is given by

$$D_i = e_{ijk}\, S_{jk} + \varepsilon_0\, \varepsilon_{ij}^{S}\, E_j\,, \tag{2}$$

where ε_0 is the electric constant and $\underline{\boldsymbol{\varepsilon}}^S$ is the dielectric tensor at constant strain, also called clamped. A different set of independent variables can be used to describe the piezoelectricity as

$$S_{ij} = s_{ijkl}^{E}\, T_{kl} + d_{kij}\, E_k \tag{3}$$

and

$$D_i = d_{ijk}\, T_{jk} + \varepsilon_0\, \varepsilon_{ij}^{T}\, E_j\,, \tag{4}$$

with the exchanged roles of stress and strain. Here $\underline{\boldsymbol{s}}^E$ is the elastic compliance tensor and $\underline{\boldsymbol{d}}$ the piezoelectric strain tensor. In the second relation we use $\underline{\boldsymbol{\varepsilon}}^T$, the dielectric tensor at zero stress (or unclamped). Depending on the experimental situation we choose the appropriate set to use. Material constants in different sets are related through thermodynamics, which gives [12]

$$\varepsilon_0 \left(\varepsilon_{ij}^{T} - \varepsilon_{ij}^{S}\right) = e_{ilm}\, d_{jlm} \tag{5}$$

and

$$e_{ijk} = C_{lmjk}^{E}\, d_{ilm}\,. \tag{6}$$

With the use of these two relations and (1)–(4), one can express the parameters from the second set (s_{ijkl}^E, d_{ijk}, and ε_{ij}^T) with parameters from the first set (C_{ijkl}^E, e_{ijk}, and ε_{ij}^S).

Until recently the basic set of elastic, dielectric, and piezoelectric parameters was to our knowledge most accurately determined in [13] from ultrasonic phase-velocity measurements and low-frequency capacitance measurements. The calculations of the basic parameters are usually based on taking differences of ultrasonic-wave velocities, which can be of comparable magnitudes; thus they are subject to rather large errors. This is the reason why some of the basic parameters listed in the literature [8, 9] differ significantly (up to 100%). Smith and Welsh [13] realised this, so they measured some uncertain parameters independently and determined the whole set of parameters iteratively. Their results are listed in the third column of Table 5. But, as was pointed out in [9], the linear hydrostatic coefficient

$$d_\mathrm{h} = 2\, d_{311} + d_{333} \tag{7}$$

was measured independently to within 1.5% to be 6.31×10^{-12} C/N [15]. The parameters obtained in [13], however, give $d_\mathrm{h} = 4.3 \times 10^{-12}$ C/N. Recently, in [14] the basic set of elastic, dielectric, and piezoelectric parameters was determined again from a very precise measurement of elastic-wave velocities, which gave $d_\mathrm{h} = 6.6 \times 10^{-12}$ C/N. However, from the 22 measured sound velocities only 10 were used for the calculation of the basic parameters.

We have taken all the measured values from [13] and [14] and calculated the basic parameters with a procedure, which will be explained later, which gave more accurate values from the same experimental results.

2.2 *Electro-optic and elasto-optic properties and material parameters*

The presence of an electric field and elastic deformations can modify the optical properties of a material. In noncentrosymmetric piezoelectric materials the induced change in the refractive index is linear in the electric field and displacement gradient and is commonly expressed by

$$\Delta\left(\frac{1}{n^2}\right)_{ij} \equiv \Delta\varepsilon_{ij}^{-1} = r_{ijk}^{S}\, E_k + p_{ijkl}^{E}\, S_{kl}\,, \tag{8}$$

where $\underline{\boldsymbol{r}}^S$ is the electro-optic tensor at zero strain (clamped) and $\underline{\boldsymbol{p}}^E$ the elasto-optic (Pockels) tensor at constant electric field. In (8) the antisymmetric contribution to the elasto-optic effect due to rotations of volume elements within elastic deformations is neglected. It can be calculated by considering [16] that in $LiNbO_3$ crystals the rotational contribution is $p_{23[23]} = p_{31[31]}$ and has a value of about $0.05\, p_{2323}^E$. As most measurements are more inaccurate, we neglect this antisymmetric term in further analysis. The Pockels tensor in $LiNbO_3$ crystals has eight independent elements; we denote them p_{1111}^E, p_{3333}^E, p_{2323}^E, p_{1122}^E, p_{1133}^E, p_{1123}^E, p_{3311}^E, and p_{2311}^E.

In an unclamped case $T_{ij} = 0$ and (3) gives $S_{ij} = d_{kij} E_k$. Inserting this into (8) we get the connection between the unclamped and the clamped electro-optic coefficients as

$$r_{ijk}^{T} = r_{ijk}^{S} + p_{ijlm}^{E}\, d_{klm}\,. \tag{9}$$

The coefficients d_{klm} can be expressed with parameters from the basic set (C_{ijkl}^E and e_{ijk}) using the thermodynamic relations. To completely describe the electro-optic and elasto-optic response in a piezoelectric crystal, we need $\underline{\boldsymbol{r}}^S$, $\underline{\boldsymbol{\varepsilon}}^S$, $\underline{\boldsymbol{p}}^E$, $\underline{\boldsymbol{C}}^E$, and $\underline{\boldsymbol{e}}$ tensor elements, which means 24 material parameters in a crystal possessing $3m$ point-group symmetry. For the calculation of sound velocities the crystal density ϱ is also needed; we consider it as an additional material parameter.

2.3 *Overview of the published data and determination of the constraints*

For the evaluation of the material parameters by a numerical procedure we have tried to use the most reliable measurements from the literature as explained later with particular data points. We calculated the basic parameters by a least-square fit approach. Each experimental result represents a constraint on the values of the material parameters. It is expressed as an algebraic function f_i of the whole set of independent material parameters, that is

$$f_i\,(a_1, \ldots, a_{25}) = y_i\,; \quad i = 1, \ldots, k\,, \tag{10}$$

where $a_1, \ldots, a_{25}$ is the chosen set of independent material parameters, y_i is the value of f_i that was determined from an experiment, and k is the number of the experimental results used in the fitting procedure. In Tables 1–4 the set of $k = 82$ measured quantities that are used is shown.

The first ten constraints in Table 1 ($i = 1, \ldots, 10$) are obtained using the thermodynamic relations (5) and (6) that give

$$s^E_{1111} = \frac{C^E_{3333}}{2\left(C^E_{3333}\left(C^E_{1111}+C^E_{1122}\right)-2\left(C^E_{1133}\right)^2\right)} - \frac{C^E_{2323}}{2\left(C^E_{2323}\left(C^E_{1122}-C^E_{1111}\right)+2\left(C^E_{1123}\right)^2\right)}, \quad (11)$$

$$d_{311} = \frac{C^E_{1133}e_{333}-C^E_{3333}e_{311}}{2\left(C^E_{1133}\right)^2-C^E_{3333}\left(C^E_{1111}+C^E_{1122}\right)}, \quad (12)$$

$$\varepsilon^T_{11} = \varepsilon^S_{11} + 2(e_{222}d_{222}+e_{113}d_{113})/\varepsilon_0, \quad (13)$$

and

$$\varepsilon^T_{33} = \varepsilon^S_{33} + (2e_{311}d_{311}+e_{333}d_{333})/\varepsilon_0, \quad (14)$$

where also the expressions for the d_{ijk} elements have to be inserted into the last two equations. The eleventh constraint is given by (7), inserting the expressions for d_{311} and d_{333} as functions of the basic set. The last four measurements in Table 1 are the crystal densities measured by different authors.

The next 35 measurements ($i = 16, \ldots, 50$) are the sound velocities, measured for different propagation and polarization directions. These directions and wave types are specified in parentheses in Table 2. The corresponding constraints are given with the solutions of the equation of motion for a displacement u_k of a volume element under the action of the internal elastic forces [12]. For plane elastic waves this equa-

i	Measured quantity	Reference	Measured value	Fitted value	Units
1	s^E_{1111}	[13]	0.5831 ± 0.006	0.5854	10^{-12} m^2/V
2	d^E_{311}	[13]	-0.0862 ± 0.0006	-0.0864	10^{-11} C/N
3	ε^T_{11}	[13]	85.13 ± 1	84.48	
4	ε^T_{11}	[14]	83.3 ± 0.8	84.48	
5	ε^T_{11}	[17]	84.6 ± 1	84.48	
6	ε^T_{33}	[13]	28.72 ± 1	27.78	
7	ε^T_{33}	[14]	28.5 ± 0.3	27.78	
8	ε^T_{33}	[17]	29.1 ± 1	27.78	
9	ε^S_{11}	[17]	44.3 ± 1	45.52	
10	ε^S_{33}	[17]	27.6 ± 1	26.22	
11	d_h	[15]	0.6310 ± 0.003	0.6346	10^{-11} C/N
12	ϱ	[13]	4640 ± 5	4643.0	kg/m^3
13	ϱ	[14]	4642.8 ± 1	4643.0	kg/m^3
14	ϱ	[18]	4646 ± 5	4643.0	kg/m^3
15	ϱ	[19]	4643 ± 3	4643.0	kg/m^3

TABLE 1 Data on dielectric constants, density, and additional elastic parameters s^E_{1111}, d^E_{311}, and d_h used in the evaluation of material constants of a $LiNbO_3$ crystal

i	Measured quantity	Reference	Measured value	Fitted value	Units
16	$v\,(x, \mathrm{T}y)$	[13]	4059.3 ± 40	4029.0	m/s
17	$v\,(x, \mathrm{T}z)$	[13]	4801.2 ± 40	4750.0	m/s
18	$v\,(y, \mathrm{L})$	[13]	6882.2 ± 40	6806.3	m/s
19	$v\,(y, \mathrm{T}x)$	[13]	3961.5 ± 40	3940.5	m/s
20	$v\,(y, \mathrm{T}z)$	[13]	4494.3 ± 40	4445.9	m/s
21	$v\,(z, \mathrm{L})$	[13]	7332.8 ± 40	7329.7	m/s
22	$v\,(z, \mathrm{T}x)$	[13]	3574.0 ± 40	3590.6	m/s
23	$v\,(y_{+40^\circ}z, \mathrm{L})$	[13]	7387.0 ± 40	7357.5	m/s
24	$v\,(y_{+40^\circ}z, \mathrm{T}x)$	[13]	4048.3 ± 40	4012.5	m/s
25	$v\,(y_{+40^\circ}z, \mathrm{T}z')$	[13]	4027.3 ± 40	4015.0	m/s
26	$v\,(y_{-40^\circ}z, \mathrm{L})$	[13]	7008.4 ± 40	6984.3	m/s
27	$v\,(y_{-40^\circ}z, \mathrm{T}x)$	[13]	3573.5 ± 40	3574.5	m/s
28	$v\,(y_{-40^\circ}z, \mathrm{T}z')$	[13]	4206.7 ± 40	4184.9	m/s
29	$v\,(y, \mathrm{L})$	[14]	6806.55 ± 0.78	6806.30	m/s
30	$v\,(y_{+32.76^\circ}z, \mathrm{L})$	[14]	7338.65 ± 0.93	7339.81	m/s
31	$v\,(y_{+58.13^\circ}z, \mathrm{L})$	[14]	7314.62 ± 0.93	7313.22	m/s
32	$v\,(z, \mathrm{L})$	[14]	7328.20 ± 0.96	7329.66	m/s
33	$v\,(y_{+147.24^\circ}z, \mathrm{L})$	[14]	6855.49 ± 0.87	6856.70	m/s
34	$v\,(x, \mathrm{L})$	[14]	6544.53 ± 0.90	6543.98	m/s
35	$v\,(y, \mathrm{T}x)$	[14]	3940.49 ± 0.63	3940.51	m/s
36	$v\,(y_{+127.85^\circ}z, \mathrm{T}x)$	[14]	3499.94 ± 0.63	3499.96	m/s
37	$v\,(z, \mathrm{T}x)$	[14]	3590.41 ± 0.69	3590.57	m/s
38	$v\,(x, \mathrm{T}z)$	[14]	4750.67 ± 1.77	4749.99	m/s
39	$v\,(y_{+9.14^\circ}z, \mathrm{L})$	[14]	6998.21 ± 1.50	6998.97	m/s
40	$v\,(y_{+68.77^\circ}z, \mathrm{L})$	[14]	7305.47 ± 1.50	7304.51	m/s
41	$v\,(y_{+77.48^\circ}z, \mathrm{L})$	[14]	7315.95 ± 1.50	7316.34	m/s
42	$v\,(y_{+107.27^\circ}z, \mathrm{L})$	[14]	7298.94 ± 1.50	7298.95	m/s
43	$v\,(y_{+127.85^\circ}z, \mathrm{L})$	[14]	7158.99 ± 1.50	7158.89	m/s
44	$v\,(y_{+162.17^\circ}z, \mathrm{L})$	[14]	6656.29 ± 1.50	6656.59	m/s
45	$v\,(x_{+15.57^\circ}z, \mathrm{L})$	[14]	6714.03 ± 1.50	6713.78	m/s
46	$v\,(x_{+29.13^\circ}z, \mathrm{L})$	[14]	6970.74 ± 1.50	6969.72	m/s
47	$v\,(x_{+39.89^\circ}z, \mathrm{L})$	[14]	7128.89 ± 1.50	7128.21	m/s
48	$v\,(x_{+48.10^\circ}z, \mathrm{L})$	[14]	7206.55 ± 1.50	7205.72	m/s
49	$v\,(x_{+65.84^\circ}z, \mathrm{L})$	[14]	7286.28 ± 1.50	7285.09	m/s
50	$v\,(x_{+100.89^\circ}y, \mathrm{L})$	[14]	6738.03 ± 1.50	6738.18	m/s

TABLE 2 Data on sound velocities used in the evaluation of material constants of a $LiNbO_3$ crystal. The sound directions and wave types are specified in *parentheses*; for example $v\,(y_{+40^\circ}z, \mathrm{L})$ indicates a longitudinal wave that propagates in the direction forming an angle $+40^\circ$ from the y axis in the crystal yz plane. For the transverse waves two possible polarization directions exist; here $v\,(y_{+40^\circ}z, \mathrm{T}z')$ indicates a (quasi)transverse wave polarized (nearly) in the direction forming an angle $+40^\circ$ from the crystal z axis

i	Measured quantity	Reference	Measured value	Fitted value	Units
51	p^E_{1111}	[20]	-0.026 ± 0.002	-0.0261	
52	p^E_{3333}	[20]	0.071 ± 0.003	0.0702	
53	p^E_{2323}	[20]	0.146 ± 0.01	0.1453	
54	p^E_{1122}	[20]	0.090 ± 0.005	0.0876	
55	p^E_{1133}	[20]	0.133 ± 0.004	0.1335	
56	p^E_{1123}	[20]	-0.075 ± 0.01	-0.0832	
57	p^E_{3311}	[20]	0.179 ± 0.01	0.1767	
58	p^E_{2311}	[20]	-0.151 ± 0.005	-0.1507	
59	p^E_{1111}	[9]	-0.032 ± 0.01	-0.0261	
60	p^E_{3333}	[9]	0.068 ± 0.005	0.702	
61	p^E_{2323}	[9]	0.148 ± 0.12	0.1453	
62	p^E_{1122}	[9]	0.081 ± 0.01	0.0876	
63	p^E_{1133}	[9]	0.135 ± 0.008	0.1335	
64	p^E_{1123}	[9]	-0.076 ± 0.02	-0.0832	
65	p^E_{3311}	[9]	0.168 ± 0.02	0.1767	
66	p^E_{2311}	[9]	-0.150 ± 0.009	-0.1507	

TABLE 3 Data on elasto-optic coefficients used in the evaluation of material constants of a $LiNbO_3$ crystal

i	Measured quantity	Reference	Measured value	Fitted value	Units
67	r^T_{113}	[21]	10.49 ± 0.4	10.12	10^{-12} m/V
68	r^T_{113}	[11]	10.0 ± 0.8	10.12	10^{-12} m/V
69	r^T_{333}	[21]	31.4 ± 1	31.45	10^{-12} m/V
70	r^T_{333}	[11]	31.5 ± 1.4	31.45	10^{-12} m/V
71	r^T_{131}	[9]	33 ± 3	33.96	10^{-12} m/V
72	r^T_{222}	[9]	6.7 ± 0.2	6.64	10^{-12} m/V
73	r^S_{113}	[22]	7.7 ± 1	9.10	10^{-12} m/V
74	r^S_{333}	[22]	28.8 ± 2	31.19	10^{-12} m/V
75	r^S_{131}	[22]	18.2 ± 1	18.09	10^{-12} m/V
76	r^S_{222}	[22]	3.4 ± 0.05	3.40	10^{-12} m/V
77	r^T_c	[23]	19.3 ± 1.0	20.1	10^{-12} m/V
78	r^T_c	[23]	21.4 ± 0.8	20.1	10^{-12} m/V
79	r^T_c	[23]	20.0 ± 0.65	20.1	10^{-12} m/V
80	r^T_c	[23]	19.7 ± 1.0	20.1	10^{-12} m/V
81	r^T_c	[23]	21.6 ± 1.2	20.1	10^{-12} m/V
82	r^T_c	[23]	19.9 ± 0.5	20.1	10^{-12} m/V

TABLE 4 Data on electro-optic coefficients used in the evaluation of material constants of a $LiNbO_3$ crystal

tion together with (1) and (2) leads to a secular equation for v^2

$$\left(\Gamma_{ik} - \delta_{ik}\varrho v^2\right) u_k = 0\,, \tag{15}$$

with

$$\Gamma_{ik} = \left(C^E_{ijkl} + \frac{e_{pij}e_{qkl}}{\left(\varepsilon^S_{rs} n_r n_s\right)} n_p n_q \right) n_j n_l\,, \tag{16}$$

where v is the wave velocity and $\hat{\boldsymbol{n}} = (n_1, n_2, n_3)$ the wave-propagation direction. The secular equation (15) yields three positive real eigenvalues ϱv^2. In a crystal possessing $3m$ symmetry and the sound propagating along the crystal y axis, for example, the solutions are one pure transverse wave with the eigenvalue

$$\varrho v^2 = \frac{1}{2}\left(C^E_{1111} - C^E_{1122}\right)\,, \tag{17}$$

one quasilongitudinal, and one quasitransverse wave. The eigenvalues for the latter two are the solutions of the quadratic equation

$$\left[\left(C^E_{1111} + e^2_{222}/\varepsilon^S_{11}\right) - \varrho v^2\right]\left[\left(C^E_{2323} + e^2_{113}/\varepsilon^S_{11}\right) - \varrho v^2\right] = \left(C^E_{1123} - e_{222}e_{113}/\varepsilon^S_{11}\right)^2\,. \tag{18}$$

Similar expressions are obtained for any other direction. The solutions for ϱv^2 in the cases of sound directed to oblique angles from crystallographic axes contain a larger number of basic parameters. The corresponding solutions give the constraints to the measured results $i = 16, \ldots, 50$ in Table 2. Equation (17), for example, gives the constraint f_{19} for $v\,(y, \mathrm{T}) = y_{19}$, while f_{18} and f_{20} are the solutions of (18).

Measurements of the elasto-optic coefficients are based on comparative Brillouin scattering of light from sound waves. We have used the results from [20], where these coefficients were determined most accurately in both magnitude and sign, also taking into account the contribution of the indirect elasto-optic effect (the combination of piezoelectric and electro-optic effects). Their results are listed in Table 3 from lines $i = 51$ to 58. We have also used the mean values for elasto-optic coefficients collected in [9] that were determined by six other authors. The mean values and the corresponding deviations are listed in Table 3 from lines $i = 59$ to 66.

The remaining part of the measurements belongs to the electro-optic coefficients and is listed in Table 4. In principle, a measurement made with an applied electric field of low frequency corresponds to the unclamped case and a measurement made with a high-frequency (rf) electric field to the clamped condition. A lot of different experimental techniques for measuring these coefficients are in use, giving results that differ by 10% in the same sample in the same opto-geometrical configuration [23]. There are, however, many recent reports on doping and stoichiometric-ratio dependences of these coefficients, also giving conflicting results, like in [24] and [25]. The stoichiometry of the crystal is determined by the crystal composition $x_c = [\mathrm{Li}]/([\mathrm{Li}] + [\mathrm{Nb}])$, where [ ] denotes the concentration in mol %. The congruent composition is defined with $x_c = 48.5\%$ and the stoichiometric one with $x_c = 50\%$. In [21] the measured r^T_{333} and r^T_{113} values were about 10% higher in an undoped congruent than in an undoped stoichiometric crystal. In [11] r^T_{113} values were almost the same for both compositions, but r^T_{333} was for about 20% higher in a stoichiometric crystal. A frequently measured quantity is the effective electro-optic coefficient $r^T_c = r^T_{333} - r^T_{113}\,(n_o/n_e)^3$. In [28] the influence of composition and iron doping on r^T_c was measured. The effective coefficient r^T_c was found to be only composition-dependent with an approximately 10% smaller value for $x_c = 49.5\%$ than for $x_c = 48.5\%$ and $x_c = 50\%$. The iron doping did not change r^T_c, but it was found to have some influence on the crystal composition. In [24], on the contrary, the coefficient r^T_{333} almost linearly increased by about 15% from $x_c = 48\%$ to $x_c = 50\%$,

while r^T_{113} remained independent of x_c. Doping with Ce or Fe also increased r^T_{333} by more than 30% [24].

For the values of r^T_{113} and r^T_{333} we have chosen results from [21], where an interferometric-type measurement of the highest accuracy was used, and the results from [11]. From both [21] and [11] data were taken for crystals of congruent composition. We have selected results for r^T_{311} and r^T_{222} by comparing different measurements in the literature [8, 9] and determining the error according to them. The clamped values of electro-optic coefficients listed in lines $i = 73, \ldots, 76$ of Table 4 are taken from [22], as they have used the refined experimental method compared to older sources of data, which are numerous. We have also taken all the results for the effective coefficient r^T_c from [23] that were obtained by different experimental techniques.

2.4 *Fitting and results*

The number of constraints $k = 82$ is larger than 25, the number of parameters; therefore it is possible to find optimum values of the parameters that fulfil the set of constraints given in Tables 1–4 by a least-square procedure. The analysis was performed using the Levenberg–Marquardt algorithm taken from [26]. This algorithm finds the set of parameters that minimises the sum χ^2 of the squared deviations of the function values $f_i\ (a_1, \ldots, a_{25})$ from the measured values y_i:

$$\chi^2 = \sum_i \frac{[f_i(a_1, \ldots, a_{25}) - y_i]^2}{(\Delta y_i)^2}, \tag{19}$$

where Δy_i is the standard deviation of the data value y_i and determines the weight of the particular measurement in the fit. The accuracies Δa_j of the parameters a_j are given by diagonal elements of the covariance matrix [26].

Measurement errors that were used in the fitting procedure and are listed in Tables 1–4 are not always given in the literature. In those cases they were determined by comparison with the results given by other authors or 'observed' behaviour during the fitting procedure.

The first twelve rows in Table 5 give our results for the elastic and dielectric constants and also repeat the corresponding values given in [13]. It is interesting to note that using the input measurements from [13] as the only data and fitting according to the first twelve parameters, χ^2 is lower when calculated from our parameters (about ten times for the accuracies listed in Table 2). The advantage of the χ-square procedure over iteration-based calculations is obvious. Some of the basic parameters are considerably changed; compare for example c^E_{1133}, e_{311}, and e_{333} values from [13] and the new fitted values. It is encouraging that our values also give a correct value for the linear hydrostatic coefficient from (7) when it is not included in the fitting procedure as a measured value.

If a value of a particular basic parameter is very stable upon changing some uncertain input data, this basic parameter is less important in the constraints and its result is more uncertain. This was typical for the eight values of the elasto-optic coefficients p^E_{ijkl} when fitting the constraints derived from the measurements of the electro-optic coefficients. The p^E_{ijkl} parameters occur only in these constraints and constraints for directly measured values. Therefore the fitted values and

TABLE 5 Basic set of the material parameters: elastic stiffness (c^E_{ijkl}), piezoelectric stress (e_{ijk}), dielectric (ε^S_{ij}), elasto-optic (p^E_{ijkl}), clamped electro-optic (r^S_{ijk}) tensor elements, and crystal density ϱ of congruent, nominally undoped $LiNbO_3$ crystal. The values given in the fourth column were determined by fitting the experimental data from Tables 1–4. All material constants are given at room temperature (25 °C) at the wavelength $\lambda_0 = 633$ nm where the refractive indices are $n_o = 2.2864$, $n_e = 2.2022$ [27]. The accuracy Δa_j of each parameter and its relative accuracy $\Delta a_j/a_j$ are listed in the fifth column. For a comparison, an older subset of the basic parameters is given in the third column

j	Parameter	Value from [13]	Fitted value a_j	Accuracy Δa_j ($\Delta a_j/a_j$)	Units
1	C^E_{1111}	2.030	1.9883	±0.0008 (0.04%)	10^{11} N/m^2
2	C^E_{1122}	0.573	0.5464	±0.0006 (0.1%)	10^{11} N/m^2
3	C^E_{1133}	0.752	0.6823	±0.0024 (0.4%)	10^{11} N/m^2
4	C^E_{1123}	0.085	0.0783	±0.0006 (0.7%)	10^{11} N/m^2
5	C^E_{3333}	2.424	2.3571	±0.002 (0.09%)	10^{11} N/m^2
6	C^E_{2323}	0.595	0.5986	±0.0003 (0.05%)	10^{11} N/m^2
7	e_{113}	3.76	3.680	±0.01 (0.3%)	C/m^2
8	e_{222}	2.43	2.424	±0.007 (0.3%)	C/m^2
9	e_{311}	0.23	0.332	±0.002 (0.7%)	C/m^2
10	e_{333}	1.33	1.785	±0.01 (0.5%)	C/m^2
11	ε^S_{11}	44.3	45.5	±0.3 (0.6%)	
12	ε^S_{33}	27.9	26.2	±0.2 (0.7%)	
13	p^E_{1111}		−0.026	±0.002 (7%)	
14	p^E_{3333}		0.070	±0.003 (4%)	
15	p^E_{2323}		0.145	±0.010 (7%)	
16	p^E_{1122}		0.088	±0.004 (5%)	
17	p^E_{1133}		0.134	±0.004 (3%)	
18	p^E_{1123}		−0.083	±0.003 (4%)	
19	p^E_{3311}		0.177	±0.009 (5%)	
20	p^E_{2311}		−0.151	±0.004 (3%)	
21	r^S_{113}		9.10	±0.3 (3%)	10^{-12} m/V
22	r^S_{333}		31.2	±0.4 (1.5%)	10^{-12} m/V
23	r^S_{131}		18.1	±1.0 (5%)	10^{-12} m/V
24	r^S_{222}		3.40	±0.05 (1.5%)	10^{-12} m/V
25	ϱ		4643.0	±0.9 (0.02%)	kg/m^3

errors remain almost unchanged from the input values $i = 51, \ldots, 58$, except in the case of p^E_{1122} and p^E_{1123} (compare Tables 3 and 5). The input values $i = 59, \ldots, 66$ are less important for the final values of the elasto-optic coefficients due to larger errors.

The results for the $\underline{\boldsymbol{r}}^S$ tensor components are listed from lines $j = 21$ to 24 in Table 5. The values for r^S_{113} and r^S_{333} are considerably changed compared to previous values (Table 4), in order to be consistent with other measurements of electro-optic coefficients.

For the fitted basic parameter values presented in Table Table 5, obtained from the measurements from Tables 1–4, the sum $\chi^2 \simeq 40$ is less than 57, which is the difference between the number of constraints and the number of parameters. As all the obtained errors are under 10%, we can have confidence in the fitted values [26] for the nominally undoped $LiNbO_3$ single crystal of congruent composition. We use these values in Sect. 3 for calculating effective coefficients for photorefractive applications of $LiNbO_3$.

3 Static dielectric constant and electro-optic effect in photorefractive experiments in $LiNbO_3$

The electric-field-induced change in the refractive index and the static dielectric response depend on the mechanical boundary conditions, either clamped or unclamped. In a photorefractive experiment, however, neither of these two cases are valid, as the deformations are in a shape of a periodic grating. The total refractive-index change is obtained by adding together the strain-free electro-optic contribution and the elasto-optic contribution, properly taking into account the rotation of the optical indicatrix axes due to shear deformations:

$$\begin{aligned}\Delta\varepsilon^{-1}_{ij} &= \left(r^S_{ijk}\hat{n}_k + p^E_{ijkl}\hat{n}_l A^{-1}_{km} B_m\right) E^{\mathrm{sc}} \cos \boldsymbol{K}\boldsymbol{r} \\ &\equiv r^{\mathrm{eff}}_{ij}\, E^{\mathrm{sc}} \cos \boldsymbol{K}\boldsymbol{r}\,, \end{aligned} \tag{20}$$

as described in [3] with an effective symmetric second-rank electro-optic tensor r^{eff}_{ij}. Tensor $\underline{\boldsymbol{A}}$ and vector $\boldsymbol{B}$ are calculated

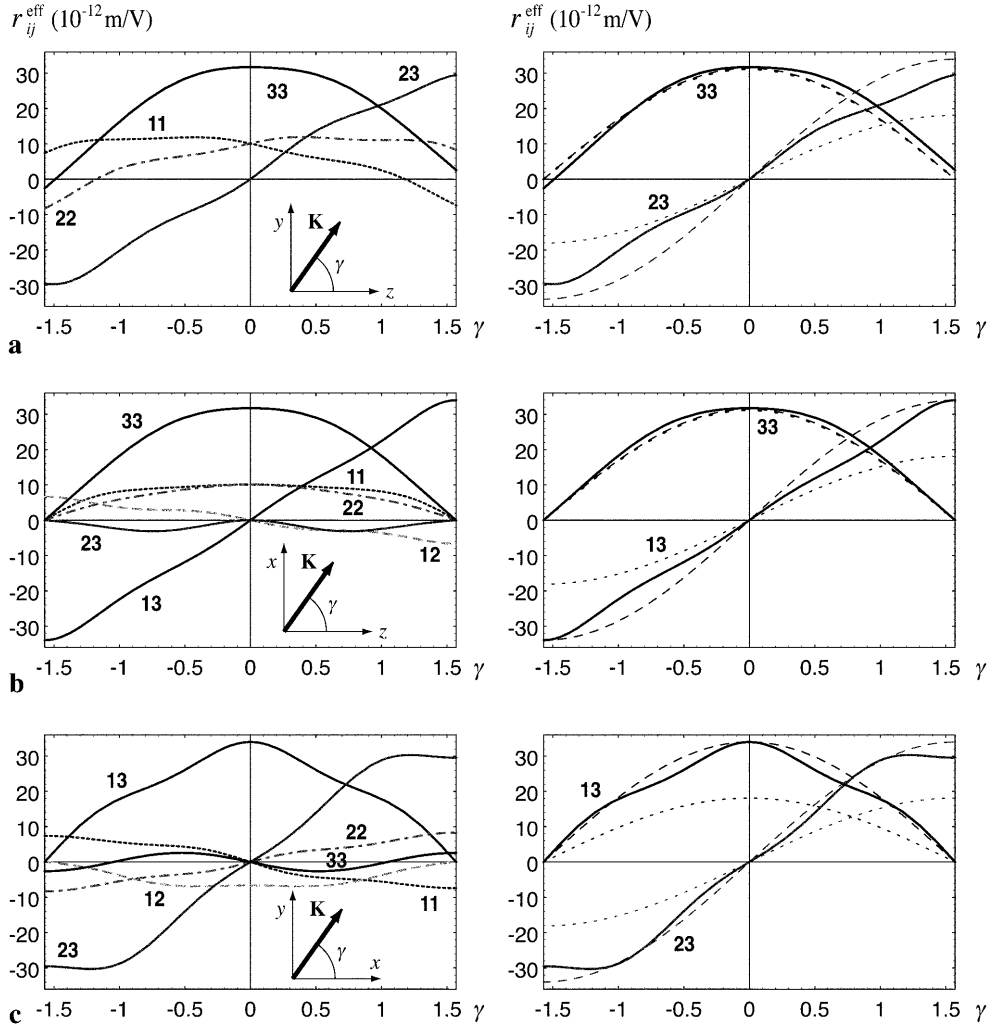

FIGURE 1 Effective electro-optic coefficients r^{eff}_{ij} defined with (20) of $LiNbO_3$ for a periodic electric field in **a** the yz plane, **b** the xz plane, and **c** the xy plane when varying the grating direction as indicated in the *insets*. The angles are given in radians throughout this work unless otherwise specified. *Left-hand graphs* show all nonzero tensor components in these planes, where for example 23 denotes $r^{\mathrm{eff}}_{23} = r^{\mathrm{eff}}_{32}$. *Right-hand graphs* show the largest two coefficients (*full lines*) and the corresponding effective coefficients in a clamped (*dotted lines*) and an unclamped (*dashed lines*) crystal subjected to a uniform electric field. Due to the small difference between r^T_{333} and r^S_{333} (see Table 4), the *dotted* and the *dashed lines* for r^{eff}_{33} are unresolvable in the plots

as

$$A_{ik} = C^{E}_{ijkl}\hat{n}_j\hat{n}_l \quad \text{and} \quad B_i = e_{kij}\hat{n}_k\hat{n}_j\,. \tag{21}$$

The values of r^{eff}_{ij} for a general direction of the electric-field grating $\hat{\boldsymbol{n}}$ can be evaluated from the whole set of relevant material parameters. With the use of parameters obtained in Sect. 2 we present the solutions for three configurations that are usually important for practical use. The result is shown in Fig. 1, where the geometry is specified – the grating wave vector in these configurations lies in either the yz plane, the xz plane, or the xy plane, respectively, and is rotated in that plane as indicated in the figure. In each plane the largest effective electro-optic coefficients are of comparable magnitude. For comparison the clamped and the unclamped dependences are also shown for some coefficients, which represent results for applying a homogeneous electric field in the same direction in strain- and stress-free mechanical conditions.

As already mentioned, the static dielectric constant is also modified due to periodic deformations. The effective dielectric constant active in photorefractive experiments is defined as in [3] to be

$$\varepsilon^{\text{eff}} = \frac{\varrho^{\text{sc}}}{\varepsilon_0 E^{\text{sc}} K} = \varepsilon^{S}_{ij}\hat{n}_i\hat{n}_j + B_k A^{-1}_{kl} B_l/\varepsilon_0\,. \tag{22}$$

Similar to the effective electro-optic tensor components, the effective dielectric constant is calculated from (22) in the same three characteristic planes. The result of the calculations is shown in Fig. 2. In photorefractive experiments, the effective dielectric constant lies between the clamped and the unclamped values $\varepsilon^{\text{eff}}_S$ and $\varepsilon^{\text{eff}}_T$.

Dependences of the effective coefficients in a periodic electric field (Figs. 1 and 2) show that the deviations from sine dependences, when considering only unclamped values, are not as large in $LiNbO_3$ as in the case of $KNbO_3$ and $BaTiO_3$ crystals [4, 6]. In $LiNbO_3$ these deviations, however, can also have a pronounced influence, as found in our preliminary experiment.

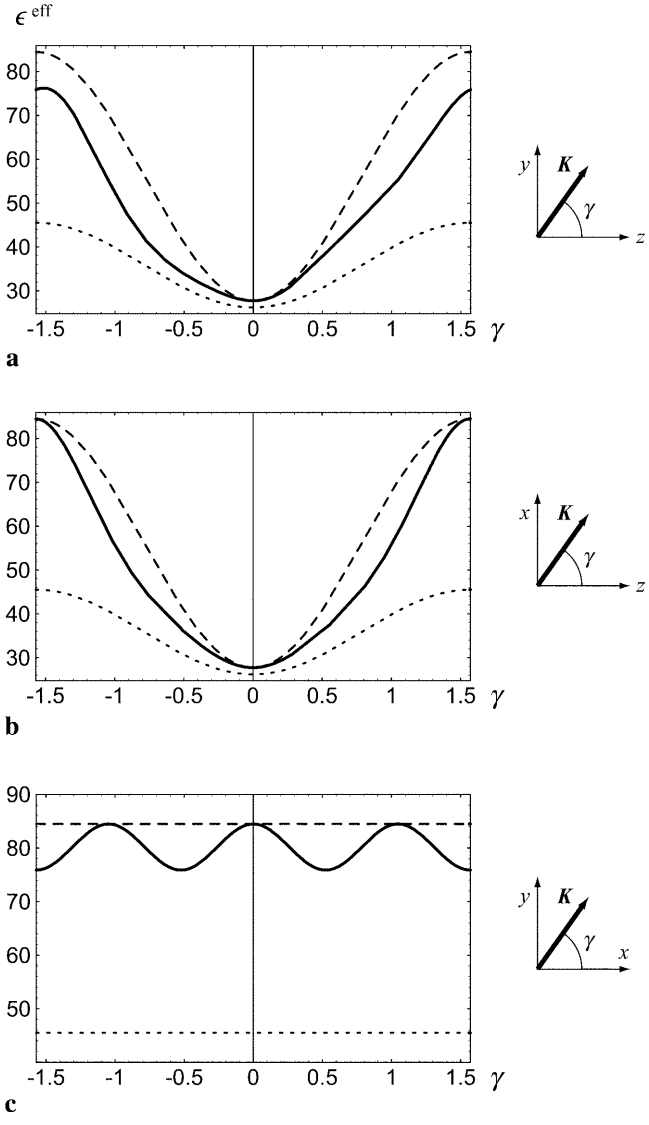

FIGURE 2 Effective dielectric constant ε^{eff} of $LiNbO_3$ in a periodic electric field in **a** the yz plane, **b** the xz plane, and **c** the xy plane (*solid lines*). For comparison, clamped (*dotted lines*) and unclamped (*dashed lines*) dependences in a uniform electric field are also shown

4 Conclusions

The complete set of material tensors of $LiNbO_3$ crystals at room temperature has been re-evaluated by a numerical fitting procedure, thus achieving considerable improvements in the accuracy of the previously published values. The parameters were determined with great confidence for nominally undoped crystals of congruent composition. Photorefractive experiments are very useful for checking the validity of the material parameters, since many of the parameters change their influence on the response by varying the orientation of the photorefractive gratings. Our preliminary experiments have confirmed that the newly determined set correctly describes the photorefractive response. Recent results on some material parameters in stoichiometric and doped $LiNbO_3$ crystals have also been reviewed. However, these results are still too incomplete to allow us to obtain a relevant model of how the doping and stoichiometry influence the material tensors.

REFERENCES

1 A.A. Izvanov, A.E. Mandel, N.D. Khat'kov, S.M. Shandarov: Optoelectronics **2**, 80 (1986)
2 G. Pauliat, M. Mathey, G. Roosen: J. Opt. Soc. Am. B **8**, 1942 (1991)
3 P. Günter, M. Zgonik: Opt. Lett. **16**, 1826 (1991)
4 M. Zgonik, K. Nakagawa, P. Günter: J. Opt. Soc. Am. B **12**, 1418 (1995)
5 G. Montemezzani: Phys. Rev. A **62**, 3803 (2000)
6 M. Zgonik, R. Schlesser, I. Biaggio, E. Voit, J. Tscherry, P. Günter: J. Appl. Phys. **74**, 1287 (1993)
7 M. Zgonik, P. Bernasconi, M. Duelli, R. Schlesser, P. Günter, M.H. Garrett, D. Rytz, Y. Zhu, X. Wu: Phys. Rev. B **50**, 5941 (1994)
8 K. Toyoda, T. Yamada: in *Landolt-Börnstein, Ferroelectrics and Related Substances*, Vol. III/16a, ed. by K.-H. Hellwege, A.M. Hellwege (Springer, Berlin 1981); M. Adachi, K. Toyoda, T. Yamada: in *Landolt-Börnstein, Ferroelectrics and Related Substances*, Vol. III/28a, ed. by T. Mitsui, E. Nakamura (Springer, Berlin 1990)
9 R.S. Weis, T.K. Gaylord: Appl. Phys. A **37**, 191 (1985)
10 A. de Bernabe, C. Prieto, A. de Andres: J. Appl. Phys. **79**, 143 (1996)
11 T. Fujiwara, M. Takahashi, M. Ohama, A.J. Ikushima, Y. Furukawa, K. Kitamura: Electron. Lett. **35**, 499 (1999)

12 J.F. Nye: *Physical Properties of Crystals* (Clarendon, Oxford 2000)
13 R.T. Smith, F.S. Welsh: J. Appl. Phys. **42**, 2219 (1971)
14 J. Kushibiki, I. Takanaga, M. Arakawa, T. Sannomiya: IEEE Trans. Ultrason. Ferroelectr. Freq. Control **46**, 1315 (1999)
15 R.A. Graham: J. Appl. Phys. **48**, 2153 (1977)
16 D.F. Nelson, M. Lax: Phys. Rev. Lett. **24**, 379 (1970)
17 A.W. Warner, M. Onoe, G.A. Coquin: J. Acoust. Soc. Am. **42**, 1223 (1967)
18 S.C. Abrahams, P. Marsh: Acta Crystallogr. **B42**, 61 (1986)
19 L. Kovács, K. Polgár: Cryst. Res. Technol. **21**, K101 (1986)
20 L.P. Avakyants, D.F. Kiselev, N.N. Shchitov: Fiz. Tverd. Tela **18**, 1547 (1976)
21 J.A. de Toro, M.D. Serrano, A. Garcia Cabanes, J.M. Cabrera: Opt. Commun. **154**, 23 (1998)
22 I.P. Kaminow, E.H. Turner, R.L. Barns, J.L. Bernstein: J. Appl. Phys. **51**, 4379 (1980)
23 M. Aillerie, N. Theofanous, M.D. Fontana: Appl. Phys. B **70**, 317 (2000)
24 Y. Kondo, T. Fukuda, Y. Yamashita, K. Yokoyama, K. Arita, M. Watanabe, Y. Furukawa, K. Kitamura, H. Nakajima: Jpn. J. Appl. Phys. **39**, 1477 (2000)
25 K. Chah, M.D. Fontana, M. Aillerie, P. Bourson, G. Malovichko: Appl. Phys. B **67**, 65 (1998)
26 W.H. Press, S.A. Teukolsky, W.T. Vetterling, B.P. Flannery: *Numerical Recipes in C, the Art of Scientific Computing*, 2nd edn. (Cambridge University Press, Cambridge, UK 1992)
27 D.E. Zelmon, D.L. Small, D. Jundt: J. Opt. Soc. Am. B **14**, 3319 (1997)
28 K. Chah, M. Aillerie, M.D. Fontana, G. Malovichko: Opt. Commun. **176**, 261 (2000)